

Quantum fluctuations can enhance or reduce positional uncertainty at finite temperature

Harukuni Ikeda*

Department of Physics, Gakushuin University, 1-5-1 Mejiro, Toshima-ku, Tokyo 171-8588, Japan

(Dated: January 29, 2025)

The uncertainty principle guarantees a non-zero value for the positional uncertainty, $\langle \Delta x^2 \rangle > 0$, even without thermal fluctuations. This implies that quantum fluctuations inherently enhance positional uncertainty at zero temperature. A natural question then arises: what happens at finite temperatures, where the interplay between quantum and thermal fluctuations may give rise to complex and intriguing behaviors? To address this question, we systematically investigate the positional uncertainty, $\langle \Delta x^2 \rangle$, of a particle in equilibrium confined within a nonlinear potential of the form $V(x) \propto x^a$, where $a = 2, 4, 6, \dots$ represents an even exponent. Using path integral Monte Carlo simulations, we calculate $\langle \Delta x^2 \rangle$ in equilibrium as a function of the thermal de Broglie wavelength Λ . Interestingly, for large values of a , $\langle \Delta x^2 \rangle$ exhibits a non-monotonic dependence on Λ : it initially decreases with increasing Λ at small Λ but increases at larger Λ . To further understand this behavior, we employ a semiclassical approximation, which reveals that quantum fluctuations can reduce positional uncertainty for small Λ when the nonlinearity of the potential is sufficiently strong. Finally, we discuss the potential implications of this result for many-body phenomena driven by strong nonlinear interactions, such as glass transitions, where the transition densities exhibit a similar non-monotonic dependence on Λ .

I. INTRODUCTION

In a classical system, the position is a deterministic variable in the absence of thermal fluctuations, *i.e.*, the positional uncertainty is zero, $\langle \Delta x^2 \rangle = 0$. In contrast, for a quantum system, the uncertainty principle ensures $\langle \Delta x^2 \rangle > 0$ [1], indicating that quantum fluctuations inherently increase positional uncertainty. What happens at finite temperatures in equilibrium? At finite temperatures, the thermal de Broglie wavelength Λ serves as a measure of the relative strength of quantum fluctuations compared to thermal fluctuations. This study systematically investigates the Λ dependence of $\langle \Delta x^2 \rangle$ in equilibrium using both numerical and theoretical approaches.

A naive intuition suggests that, at a fixed temperature, $\langle \Delta x^2 \rangle$ should increase with increasing Λ , owing to tunneling effects and zero-point energy [1]. This intuition holds true in the simplest case: a particle confined in a harmonic potential, $V(x) \propto x^2$, where $\langle \Delta x^2 \rangle$ increases monotonically as Λ increases [2]. However, this behavior does not generalize to all systems, as seen in another analytically solvable example: a particle confined between hard walls. For a classical particle at finite temperature, the positional distribution is uniform between the walls. In contrast, for finite Λ , quantum effects become significant. The boundary conditions and the continuity of the wave function suppress the probability of finding the particle near the walls. As a result, $\langle \Delta x^2 \rangle$ becomes smaller than its classical counterpart ($\Lambda = 0$), demonstrating that quantum fluctuations can suppress positional uncertainty.

The observation that quantum fluctuations can suppress positional uncertainty is rather counterintuitive.

Interestingly, similar behaviors have been reported in many-body quantum systems. For example, quantum fluctuations often reduce the uncertainty in the rotational degrees of freedom of hydrogen molecules in solid phases, which stabilizes the so-called phase II (the partially frozen phase) [3–5]. Related phenomena have also been observed in crystallization [6–11], glass transitions [12–19], and spin-glass transitions [20–23], where quantum fluctuations reduce the transition densities. An intuitive explanation for these phenomena is that quantum fluctuations effectively increase the particles' radii, thereby reducing the accessible volume and lowering the transition density [12, 13]. This situation is analogous to the case of a single particle confined between hard walls, where quantum fluctuations, as described earlier, prevent the particle from occupying regions near the walls. This effectively reduces the accessible volume.

An important and natural question is: under what conditions do quantum fluctuations suppress positional uncertainty? To address this question, we systematically study a particle confined in a nonlinear potential, $V(x) \propto x^a$, where $a = 2, 4, \dots$ represents an even number. By varying a , we can systematically change the functional form from harmonic ($a = 2$) to hard walls ($a \rightarrow \infty$).

We investigate the model for $2 < a < \infty$ using path-integral Monte Carlo simulations [24–27]. For weakly nonlinear potentials (*i.e.*, small a), $\langle \Delta x^2 \rangle$ increases monotonically with increasing Λ , similar to the behavior observed in the harmonic potential case. Interestingly, for large a , $\langle \Delta x^2 \rangle$ decreases from its classical value at moderate Λ , indicating that quantum fluctuations suppress the positional uncertainty. This effect becomes most pronounced in the hard-wall limit ($a \rightarrow \infty$), where $\langle \Delta x^2 \rangle$ decreases monotonically with Λ . To further understand this behavior, we perform a semi-classical cal-

* harukuni.ikeda@gakushuin.ac.jp

ulation [24, 28] to determine the conditions under which quantum fluctuations suppress $\langle \Delta x^2 \rangle$. The semi-classical analysis predicts that $\langle \Delta x^2 \rangle$ increases for $a = 2, 4$ and decreases for $a > 4$ at small Λ , consistent with the numerical results. These findings demonstrate that quantum fluctuations can generally suppress positional uncertainty at small Λ when the potential is strongly nonlinear.

The structure of the paper is as follows. In Sec.II, we introduce the model. In Sec.III, we briefly review two analytically solvable cases: the harmonic potential and hard walls. In Sec.IV, we present the numerical results obtained through path-integral Monte Carlo simulations. In Sec.V, we provide analytical insights derived from the semi-classical calculation. Finally, Sec. VI is dedicated to the summary and discussions, highlighting some potential implications of our findings for studies of glass transitions.

II. SETTINGS

In this section, we introduce the model and define key physical quantities.

A. Model

We consider a particle in one dimension confined within a potential $V(x)$. The Hamiltonian of the system is given by:

$$H = \frac{p^2}{2m} + V(x), \quad (1)$$

where the potential $V(x)$ is defined as:

$$V(x) = k \left(\frac{x}{L} \right)^a, \quad (2)$$

with $a = 2, 4, 6, \dots$ representing an even number. The position x and momentum p satisfy the canonical commutation relation [1]:

$$[x, p] = i\hbar. \quad (3)$$

For $a = 2$, $V(x)$ corresponds to a harmonic potential, while in the limit $a \rightarrow \infty$, it approaches the case of hard walls, as shown in Fig. 1.

To quantify the positional uncertainty, we observe the variance of x in equilibrium:

$$\langle \Delta x^2 \rangle \equiv \frac{1}{Z} \text{Tr} (e^{-\beta H} x^2), \quad Z = \text{Tr} e^{-\beta H}, \quad (4)$$

where $\beta = 1/(k_B T)$ is the inverse temperature, and k_B is the Boltzmann constant.

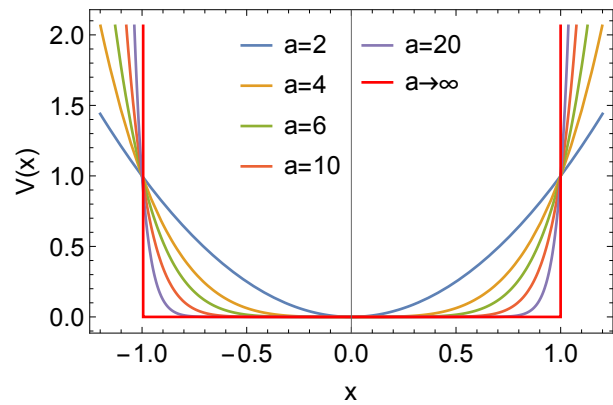


FIG. 1. Potentials for several values of a . The potential is harmonic when $a = 2$, and it becomes equivalent to hard walls in the limit $a \rightarrow \infty$. For simplicity, we set $k = 1$ and $L = 1$ in this figure.

B. Nondimensionalization

We introduce dimensionless variables:

$$\tilde{x} = L^{-1}x, \quad \tilde{p} = \frac{L}{\hbar}p, \quad (5)$$

which satisfy the commutation relation:

$$[\tilde{x}, \tilde{p}] = i. \quad (6)$$

With these dimensionless quantities, the partition function can be rewritten as:

$$Z = \text{Tr} \exp \left[-\Lambda^2 \frac{\tilde{p}^2}{2} - \tilde{\beta} \tilde{V}(\tilde{x}) \right], \quad (7)$$

where:

$$\Lambda = \sqrt{\frac{\beta \hbar^2}{mL^2}}, \quad \tilde{\beta} = k\beta, \quad \tilde{V}(\tilde{x}) = |\tilde{x}|^a. \quad (8)$$

After nondimensionalization, the system is governed by two control parameters: the reduced inverse temperature $\tilde{\beta}$ and the thermal de Broglie wavelength Λ [2].

III. SOLVABLE CASES

Here we shortly revisit the well known solvable cases.

A. Analytical Results for $a = 2$ (Harmonic Potential)

The model can be solved analytically for $a = 2$, where $V(x)$ is a harmonic potential. In this case, the equilibrium distribution of \tilde{x} follows a Gaussian distribution [2, 29]:

$$\rho(\tilde{x}) = \frac{1}{Z} \langle \tilde{x} | e^{-\beta H} | \tilde{x} \rangle = \frac{1}{\sqrt{2\pi \langle \Delta \tilde{x}^2 \rangle}} e^{-\frac{\tilde{x}^2}{2 \langle \Delta \tilde{x}^2 \rangle}}, \quad (9)$$

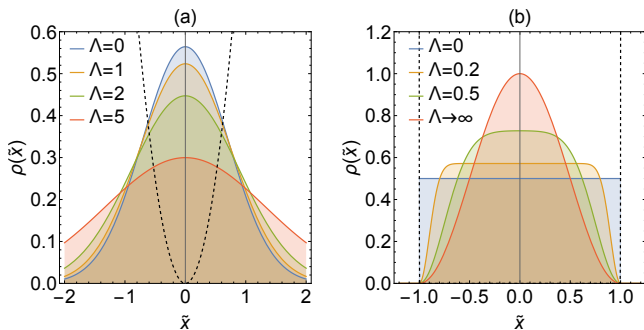


FIG. 2. Equilibrium distributions $\rho(\tilde{x})$ for $\tilde{\beta} = 1$. (a) $\rho(\tilde{x})$ for $a = 2$ (harmonic potential). Solid lines represent $\rho(\tilde{x})$ for various values of the de Broglie wave lengths $\Lambda = \sqrt{\frac{\beta\hbar^2}{mL^2}}$, while the black dashed line represents the potential $V(\tilde{x}) = \tilde{x}^2$. The distribution $\rho(\tilde{x})$ widens as Λ increases. (b) Same plots for the limit $a \rightarrow \infty$ (hard walls). In this case, the distribution becomes narrower as Λ increases.

where the variance is given by:

$$\langle \Delta \tilde{x}^2 \rangle = \frac{\Lambda}{2\sqrt{2\tilde{\beta}}} \coth \left(\Lambda \sqrt{\frac{\tilde{\beta}}{2}} \right). \quad (10)$$

As shown in Fig. 2 (a), the distribution $\rho(\tilde{x})$ broadens with increasing Λ , indicating that quantum fluctuations enhance the positional uncertainty. This result is expected, as tunneling effects and zero-point energy weaken the confinement imposed by the potential. In Fig. 3, we plot $\langle \Delta \tilde{x}^2 \rangle$ as the blue solid line, showing its monotonic increase with Λ .

B. Analytical Results for $a \rightarrow \infty$ (Hard Walls)

In the limit $a \rightarrow \infty$, the model corresponds to a particle confined between hard walls at $\tilde{x} = \pm 1$. For the classical case $\Lambda = 0$, the equilibrium distribution is flat:

$$\lim_{\Lambda \rightarrow 0} \rho(\tilde{x}) = \begin{cases} 1/2 & |\tilde{x}| < 1, \\ 0 & |\tilde{x}| \geq 1, \end{cases} \quad (11)$$

which results in a positional uncertainty:

$$\langle \Delta \tilde{x}^2 \rangle_0 = \frac{1}{3}. \quad (12)$$

For $\Lambda > 0$, the equilibrium distribution is expressed as:

$$\rho(\tilde{x}) = \frac{1}{Z} \sum_{n=1}^{\infty} e^{-\frac{(n\pi\Lambda)^2}{8}} |\phi_n(\tilde{x})|^2, \quad Z = \sum_{n=1}^{\infty} e^{-\frac{(n\pi\Lambda)^2}{8}}, \quad (13)$$

where $\phi_n(\tilde{x})$ denotes the n -th eigenfunction:

$$\phi_n(\tilde{x}) = \sin \left(n\pi \frac{\tilde{x} - 1}{2} \right). \quad (14)$$

Due to the boundary conditions $\phi_n(\tilde{x} = \pm 1) = 0$ and the continuity of the wave function, the eigenfunctions' amplitudes are significantly suppressed near the walls, $|\phi_n(\tilde{x})| \ll 1$ for $|\tilde{x}| \approx 1$. This results in a narrower distribution of $\rho(\tilde{x})$ compared to the classical case, as shown in Fig. 2 (b). In the limit $\Lambda \rightarrow \infty$, the distribution converges to that of the ground state:

$$\lim_{\Lambda \rightarrow \infty} \rho(\tilde{x}) = \left| \sin \left(\pi \frac{\tilde{x} - 1}{2} \right) \right|^2, \quad (15)$$

which results in the positional uncertainty:

$$\langle \Delta \tilde{x}^2 \rangle_{\infty} = \frac{1}{3} - \frac{2}{\pi^2}. \quad (16)$$

In Fig. 3, we plot $\langle \Delta \tilde{x}^2 \rangle = \int d\tilde{x} \rho(\tilde{x}) \tilde{x}^2$ as the red solid line. The positional uncertainty $\langle \Delta \tilde{x}^2 \rangle$ monotonically decreases with Λ from $\langle \Delta \tilde{x}^2 \rangle_0$ to $\langle \Delta \tilde{x}^2 \rangle_{\infty}$.

IV. NUMERICAL SIMULATION

For $2 < a < \infty$, the model cannot be solved analytically. In this section, we present the numerical results for these cases.

A. Path Integral Formulation

To investigate the model numerically, we reformulate the partition function Z using the path-integral formalism [24, 25, 27, 30]:

$$Z = \lim_{N \rightarrow \infty} \left(\frac{N}{2\pi\Lambda^2} \right)^{N/2} \left(\prod_{i=1}^N \int d\tilde{x}_i \right) \exp \left[-\tilde{\beta} \Phi(\tilde{x}_1, \dots, \tilde{x}_N) \right], \quad (17)$$

where we introduce the effective potential:

$$\Phi(\tilde{x}_1, \dots, \tilde{x}_N) = \sum_{i=1}^N \left[\frac{N}{2\tilde{\beta}\Lambda^2} (\tilde{x}_{i+1} - \tilde{x}_i)^2 \frac{\tilde{V}(\tilde{x}_i)}{N} \right]. \quad (18)$$

The thermal average of a physical quantity $A(\tilde{x})$ can then be expressed as [25]:

$$\langle A(\tilde{x}) \rangle = \lim_{N \rightarrow \infty} \frac{1}{N} \sum_{i=1}^N \langle A(\tilde{x}_i) \rangle, \quad (19)$$

where $\langle \bullet \rangle$ denotes the thermal average over the equilibrium configurations under the effective potential Φ .

B. Details of Numerical Implementation

We sample the equilibrium configurations $\tilde{x}_1, \dots, \tilde{x}_N$ using Monte Carlo (MC) simulations with the effective

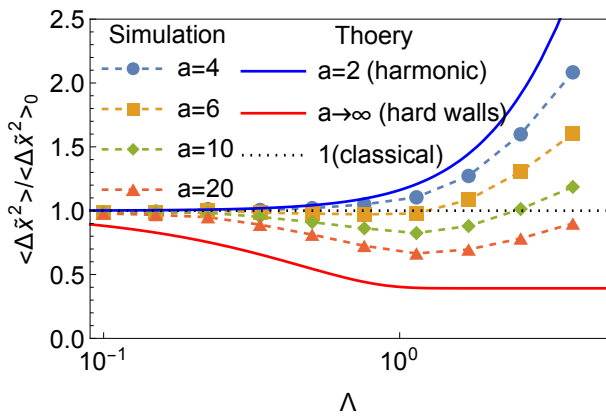


FIG. 3. Thermal de Broglie wavelength $\Lambda = \sqrt{\frac{\beta \hbar^2}{mL^2}}$ dependence of $\langle \Delta \tilde{x}^2 \rangle$, normalized by the classical result $\langle \Delta \tilde{x}^2 \rangle_0$. Here, we set $\tilde{\beta} = 1$. Markers indicate numerical results for $a = 2, \dots, 20$, and solid lines represent analytical results for $a = 2$ and $a \rightarrow \infty$. The black dotted line corresponds to $\langle \Delta \tilde{x}^2 \rangle / \langle \Delta \tilde{x}^2 \rangle_0 = 1$. For $a = 2$ and 4 , $\langle \Delta \tilde{x}^2 \rangle$ increases monotonically, while for $a = 6, 10$, and 20 , $\langle \Delta \tilde{x}^2 \rangle$ decreases for small Λ and increases for large Λ . See Fig. 5 for an enlarged view of the data for small Λ .

potential Φ in Eq. (18). A single MC step involves N local updates of $\tilde{x}_i \rightarrow \tilde{x}_i + \delta_x$ for a randomly chosen i , along with a center-of-mass update $R \rightarrow R + \delta_R$ to accelerate relaxation. Here, δ_x and δ_R are small random numbers with $\delta_x \in [-0.05\Lambda, 0.05\Lambda]$ and $\delta_R \in [-0.05, 0.05]$. Each update is accepted with probability $\min[1, e^{-\tilde{\beta}\Delta\Phi}]$, where $\Delta\Phi$ represents the energy change caused by the update. In this study, we present results for $N = 50$. Simulations with $N = 100$ were also performed to confirm that the results are independent of N . We equilibrated the system using 10^7 MC steps, followed by an additional 10^7 steps to compute the thermal average of $\langle \Delta \tilde{x}^2 \rangle$.

C. Results

Fig. 3 summarizes our numerical results for various values of a . For small a ($a = 2$ and 4), $\langle \Delta \tilde{x}^2 \rangle$ increases monotonically with Λ , indicating that quantum fluctuations enhance positional uncertainty. In contrast, for larger a ($a = 6, 10$, and 20), $\langle \Delta \tilde{x}^2 \rangle$ exhibits non-monotonic behavior: it decreases for small Λ and increases for large Λ . These results suggest that quantum fluctuations can reduce positional uncertainty for small Λ . Interestingly, similar non-monotonic behaviors have been reported in previous studies of the glass transitions [12, 14].

V. SEMI-CLASSICAL APPROXIMATION

We employ the semi-classical approximation to get a physical insight into the non-monotonic behavior for large a and small Λ . Notably, the decreases of $\langle \Delta \tilde{x}^2 \rangle$ occur for small Λ , allowing us to determine whether $\langle \Delta \tilde{x}^2 \rangle$ decreases or not by analyzing the sign of the leading-order correction in the semi-classical approximation [15, 24].

A. Partition function

We begin by decomposing \tilde{x}_i into a center-of-mass term and fluctuations:

$$\tilde{x}_i = R + u_i, \quad (20)$$

where $R = N^{-1} \sum_{i=1}^N \tilde{x}_i$ represents the center-of-mass, and u_i are fluctuations around it. For $\Lambda \ll 1$, the fluctuations are small, $|u_i| \ll 1$, enabling an expansion of $\tilde{V}(\tilde{x}_i)$ around R . The partition function then becomes:

$$Z \approx \lim_{N \rightarrow \infty} \left(\frac{N}{2\pi\Lambda^2} \right)^{N/2} \int dR \prod_{i=1}^N \int du_i \delta \left(N^{-1} \sum_i u_i \right) \times e^{-\frac{N}{2\Lambda^2} \sum_{i=1}^N (u_{i+1} - u_i)^2 - \tilde{\beta} \tilde{V}(R) - \frac{\tilde{\beta} \tilde{V}''(R)}{2N} \sum_i u_i^2}. \quad (21)$$

After integrating out the Gaussian fluctuations u_i , the partition function reduces to [24, 28]

$$Z \propto \int dR \exp \left[-\tilde{\beta} \tilde{V}_{\text{eff}}(R) \right], \quad (22)$$

where the effective potential is given by

$$\tilde{V}_{\text{eff}}(R) = \tilde{V}(R) + \frac{\Lambda^2}{24} \tilde{V}''(R). \quad (23)$$

The above equation implies that the distribution of the center-of-mass can be identified with that of a classical particle confined in the effective potential Eq. (23) at the level of the semi-classical approximation [24, 28].

B. Positional uncertainty

The positional uncertainty can be written as

$$\langle \Delta \tilde{x}^2 \rangle = \langle R^2 \rangle + \lim_{N \rightarrow \infty} \frac{1}{N} \sum_{i=1}^N \langle u_i^2 \rangle. \quad (24)$$

The first term in Eq. (24) is approximated as

$$\begin{aligned} \langle R^2 \rangle &\approx \frac{\int dR e^{-\tilde{\beta} \tilde{V}_{\text{eff}}(R)} R^2}{\int dR e^{-\tilde{\beta} \tilde{V}_{\text{eff}}(R)}} \\ &\approx \langle R^2 \rangle_0 - \frac{\Lambda^2}{24} \left[\langle \tilde{V}''(R) R^2 \rangle_0 - \langle \tilde{V}''(R) \rangle_0 \langle R^2 \rangle_0 \right], \end{aligned} \quad (25)$$

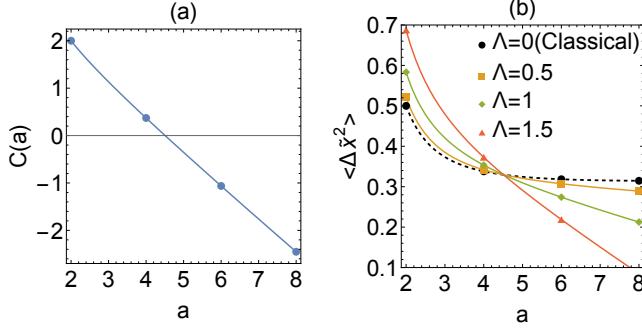


FIG. 4. Results of the semi-classical approximation. (a) Coefficient of the leading-order quantum correction, $C(a)$. The coefficient is positive ($C(a) > 0$) for $a = 2$ and 4 , while it becomes negative ($C(a) < 0$) for $a > 4$. Note that $C(a)$ is independent of the reduced temperature $\tilde{\beta}$. (b) Positional uncertainty $\langle \Delta \tilde{x}^2 \rangle$ for $\tilde{\beta} = 1$ as a function of Λ for various values of a . For $a = 2$ and 4 , $\langle \Delta \tilde{x}^2 \rangle$ increases with increasing Λ , indicating that quantum fluctuations enhance the positional uncertainty. In contrast, for $a > 4$, $\langle \Delta \tilde{x}^2 \rangle$ decreases with increasing Λ , demonstrating the suppression of positional uncertainty by quantum fluctuations.

where $\langle \bullet \rangle_0 = \langle \bullet \rangle|_{\Lambda=0}$ denotes the classical equilibrium average for $\Lambda = 0$:

$$\langle \bullet \rangle_0 = \frac{\int dR e^{-\tilde{\beta}\tilde{V}(R)} \bullet}{\int dR e^{-\tilde{\beta}\tilde{V}(R)}}. \quad (26)$$

Since $\langle \tilde{V}''(R)R^2 \rangle_0 \geq \langle \tilde{V}''(R) \rangle_0 \langle R^2 \rangle_0$, the $O(\Lambda^2)$ order term in Eq. (25) always give negative contribution, which reduces the positional uncertainty $\langle \Delta \tilde{x}^2 \rangle$. Note that this term appears only for non-linear potentials since the $O(\Lambda^2)$ order term in Eq. (25) vanishes for the harmonic potential $\tilde{V}(R) = R^2$. The second term in Eq. (24) is calculated as [24]

$$\lim_{N \rightarrow \infty} \frac{1}{N} \sum_{i=1}^N \langle u_i^2 \rangle \approx \frac{\Lambda^2}{12}, \quad (27)$$

which gives a positive contribution and enhances the positional uncertainty. Due to the competition of the terms in Eq. (25) and (27), the least-order contribution changes the sign at a certain value of a , which determines whether $\langle \Delta \tilde{x}^2 \rangle$ increase or decrease for small Λ .

For the potential $\tilde{V}(\tilde{x}) = \tilde{x}^a$, we get

$$\langle \Delta \tilde{x}^2 \rangle \approx \langle \Delta \tilde{x}^2 \rangle_0 + \frac{\Lambda^2}{24} C(a), \quad (28)$$

where

$$\langle \Delta \tilde{x}^2 \rangle_0 = \tilde{\beta}^{-2/a} \frac{\Gamma(3/a)}{\Gamma(1/a)}, \quad (29)$$

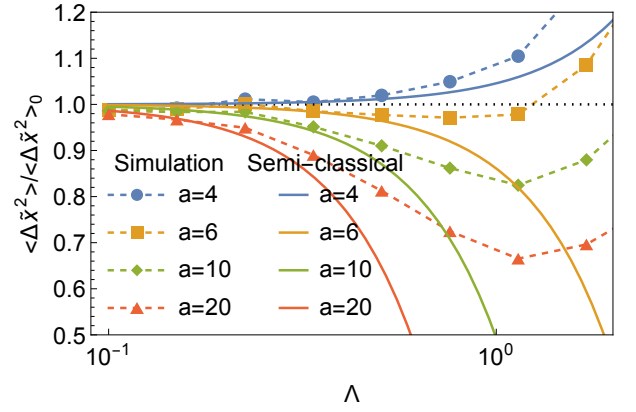


FIG. 5. Comparison between numerical simulations and semi-classical calculations for $\tilde{\beta} = 1$. Markers represent the same numerical results as in Fig. 3, while solid lines indicate the results of the semi-classical approximation. The numerical and theoretical results agree well for small Λ , accurately capturing the initial trends in $\langle \Delta \tilde{x}^2 \rangle$. However, the results diverge for large Λ , where higher-order corrections become significant.

and

$$\begin{aligned} C(a) &= 2 - \left(\langle \tilde{V}''(R)R^2 \rangle_0 - \langle \tilde{V}''(R) \rangle_0 \langle R^2 \rangle_0 \right), \\ &= 2 - a(a-1) \left(\frac{\Gamma(\frac{1+a}{a})}{\Gamma(\frac{1}{a})} - \frac{\Gamma(\frac{3}{a})\Gamma(\frac{a-1}{a})}{\Gamma(\frac{1}{a})^2} \right). \end{aligned} \quad (30)$$

As shown in Fig. 4 (a), the coefficient $C(a)$ is positive for $a = 2$ and 4 , but becomes negative for $a > 4$. For $a = 2$ and 4 , the positive contribution increases $\langle \Delta \tilde{x}^2 \rangle$ with Λ , indicating that quantum fluctuations enhance the positional uncertainty, as illustrated in Fig. 4 (b). In contrast, for $a > 4$, quantum fluctuations suppress the positional uncertainty at small Λ , as seen in Fig. 4 (b). Note that this trend is independent of the temperature for the current model, as $C(a)$ does not explicitly involve $\tilde{\beta}$. However, for more general potential shapes, the sign of the leading-order correction may depend on $\tilde{\beta}$, introducing a possible temperature dependence.

In Fig. 5, we compare the semi-classical result, Eq.(28), with the numerical results. The semi-classical approximation agrees well with the numerical results for small Λ , particularly in capturing the initial increase or decrease of $\langle \Delta \tilde{x}^2 \rangle$. However, higher-order corrections become significant for large Λ , invalidating the semi-classical approximation. Notably, the semi-classical calculation fails to reproduce the non-monotonic behavior of $\langle \Delta \tilde{x}^2 \rangle$ observed for $a > 4$. This is expected, as the semi-classical approximation considers only the $O(\Lambda^2)$ terms, which can describe only monotonic increases or decreases in $\langle \Delta \tilde{x}^2 \rangle$. Higher-order corrections are necessary to fully account for the non-monotonic behavior, which we leave as future work.

VI. SUMMARY AND DISCUSSIONS

In summary, we have investigated the effects of quantum fluctuations on the positional uncertainty $\langle \Delta x^2 \rangle$ of a particle confined in a non-linear potential, $V(x) = kx^a$. Our results demonstrate that quantum fluctuations suppress $\langle \Delta x^2 \rangle$ for sufficiently strong non-linear potentials and small de Broglie wavelengths Λ . For larger Λ , tunneling effects dominate, leading to an increase in $\langle \Delta x^2 \rangle$ and resulting in a non-monotonic dependence of $\langle \Delta x^2 \rangle$ on Λ .

The phenomena observed in our single-particle model may also be relevant to many-body quantum systems. For instance, previous studies have reported that quantum fluctuations enhance crystallization [6–11] and vitrification [12–19] for small Λ . An intuitive explanation for these observations is that quantum fluctuations effectively increase the particle radius, thereby reducing the free volume [12, 13]. This mechanism resembles the behavior observed in our model, where quantum fluctuations reduce $\langle \Delta x^2 \rangle$ for sufficiently strong non-linear potentials and small Λ , indicating stronger confinement of the particle within a narrower region and a corresponding reduction in free volume. Moreover, the non-monotonic Λ dependence of $\langle \Delta x^2 \rangle$ observed in Fig.3 is reminiscent of the non-monotonic behavior of the glass transition point reported in previous studies[12]. These similarities suggest that our model may provide a minimal framework for understanding the non-monotonic behavior observed in studies of glass transitions [12, 13]. However, it is important to note that our study focuses on a single-particle system, whereas glass transitions involve many-body interactions. Further studies are needed to establish a more direct connection between these problems.

In the hard-wall limit ($a \rightarrow \infty$), $\langle \Delta x^2 \rangle$ monotonically

decreases with increasing Λ . This behavior contrasts with predictions from mode-coupling theory (MCT), a dynamical mean-field theory of glass transitions [31–33], which suggests a non-monotonic dependence of the glass transition point on Λ even for hard-sphere potentials [12, 14]. Recently, an exact calculation for quantum hard spheres has been performed in the limit of large spatial dimensions [19], using the replica liquid theory (RLT), a static mean-field theory of glass transitions [34–39]. The RLT predicts a monotonic decrease of the glass transition point with increasing Λ , which is qualitatively consistent with our findings in the hard-wall limit. Additionally, studies on the crystallization of quantum hard spheres have consistently reported a monotonic decrease in the transition point with increasing Λ [6–10]. This consistency leads us to speculate that the non-monotonic behavior predicted by MCT for quantum hard spheres may be an artifact of the approximation. Further investigations would be valuable to clarify this point.

ACKNOWLEDGMENTS

We thank A. Ikeda, M. Udagawa, and K. Miyazaki, for helpful discussions. I acknowledge the use of OpenAI’s ChatGPT (<https://chat.openai.com/>) for assistance in improving the clarity, grammar, and overall readability of the manuscript. This work was supported by KAKENHI 23K13031.

DATA AVAILABILITY

The data that support the findings of this study are available from the corresponding author upon reasonable request.

-
- [1] W. Greiner, *Quantum mechanics: an introduction* (Springer Science & Business Media, 2011).
- [2] W. Greiner, L. Neise, and H. Stöcker, *Thermodynamics and statistical mechanics* (Springer Science & Business Media, 2012).
- [3] H. Kitamura, S. Tsuneyuki, T. Ogitsu, and T. Miyake, *Nature* **404**, 259 (2000).
- [4] R. J. Hemley, *Nature* **404**, 240 (2000).
- [5] S. Tsuneyuki, *Current Opinion in Solid State and Materials Science* **6**, 147 (2002).
- [6] J.-P. Hansen, D. Levesque, and D. Schiff, *Phys. Rev. A* **3**, 776 (1971).
- [7] K. J. Runge and G. V. Chester, *Phys. Rev. B* **38**, 135 (1988).
- [8] L. M. Sesé, *The Journal of chemical physics* **126** (2007).
- [9] L. M. Sesé and L. E. Bailey, *The Journal of chemical physics* **126** (2007).
- [10] L. M. Sesé, *The Journal of Chemical Physics* **139** (2013).
- [11] K. Yamashita, Y. Kwon, Y. Koike, and D. S. Hirashima, *Journal of the Physical Society of Japan* **83**, 043602 (2014).
- [12] T. E. Markland, J. A. Morrone, B. J. Berne, K. Miyazaki, E. Rabani, and D. R. Reichman, *Nature Physics* **7**, 134–137 (2011).
- [13] F. Zamponi, *Nature Physics* **7**, 99–100 (2011).
- [14] T. E. Markland, J. A. Morrone, K. Miyazaki, B. J. Berne, D. R. Reichman, and E. Rabani, *The Journal of Chemical Physics* **136** (2012), 10.1063/1.3684881.
- [15] G. Biroli and F. Zamponi, *Journal of Low Temperature Physics* **168**, 101 (2012).
- [16] K. Kinugawa and A. Takemoto, *The Journal of Chemical Physics* **154** (2021), 10.1063/5.0048539.
- [17] A. Das, E. Rabani, K. Miyazaki, and U. Harbola, *The Journal of Chemical Physics* **154** (2021), 10.1063/5.0032085.
- [18] A. Das, G. Krishnan, E. Rabani, and U. Harbola, *Phys. Rev. E* **105**, 054136 (2022).
- [19] M. Winer, C. L. Baldwin, R. Barney, V. Galitski, and B. Swingle, *Phys. Rev. E* **109**, 044112 (2024).
- [20] L. Foini, G. Semerjian, and F. Zamponi, *Phys. Rev. Lett.* **105**, 167204 (2010).

- [21] L. Foini, G. Semerjian, and F. Zamponi, *Phys. Rev. B* **83**, 094513 (2011).
- [22] S. J. Thomson, P. Urbani, and M. Schiró, *Phys. Rev. Lett.* **125**, 120602 (2020).
- [23] P. Urbani, *Journal of Statistical Mechanics: Theory and Experiment* **2024**, 083301 (2024).
- [24] R. P. Feynman, A. R. Hibbs, and D. F. Styer, *Quantum mechanics and path integrals* (Courier Corporation, 2010).
- [25] M. E. Tuckerman, B. J. Berne, G. J. Martyna, and M. L. Klein, *The Journal of Chemical Physics* **99**, 2796–2808 (1993).
- [26] D. M. Ceperley, *Rev. Mod. Phys.* **67**, 279 (1995).
- [27] S. Habershon, D. E. Manolopoulos, T. E. Markland, and T. F. Miller III, *Annual review of physical chemistry* **64**, 387 (2013).
- [28] J. Zinn-Justin, *Quantum field theory and critical phenomena*, Vol. 171 (Oxford university press, 2021).
- [29] K. Schönhammer, *American Journal of Physics* **82**, 887–895 (2014).
- [30] S. Mittal, M. J. Westbroek, P. R. King, and D. D. Vvedensky, *European Journal of Physics* **41**, 055401 (2020).
- [31] W. Götze, *Journal of Physics: condensed matter* **11**, A1 (1999).
- [32] D. R. Reichman and P. Charbonneau, *Journal of Statistical Mechanics: Theory and Experiment* **2005**, P05013 (2005).
- [33] W. Götze, *Complex dynamics of glass-forming liquids: A mode-coupling theory*, Vol. 143 (Oxford University Press, USA, 2009).
- [34] S. F. Edwards and P. W. Anderson, *Journal of Physics F: Metal Physics* **5**, 965–974 (1975).
- [35] M. Mézard, G. Parisi, and M. A. Virasoro, *Spin glass theory and beyond: An Introduction to the Replica Method and Its Applications*, Vol. 9 (World Scientific Publishing Company, 1987).
- [36] M. Mézard and G. Parisi, *The Journal of chemical physics* **111**, 1076 (1999).
- [37] P. Charbonneau, J. Kurchan, G. Parisi, P. Urbani, and F. Zamponi, *Annual Review of Condensed Matter Physics* **8**, 265 (2017).
- [38] G. Parisi and F. Zamponi, *Rev. Mod. Phys.* **82**, 789 (2010).
- [39] G. Parisi, P. Urbani, and F. Zamponi, *Theory of simple glasses: exact solutions in infinite dimensions* (Cambridge University Press, 2020).